

2P and 4P C II photoabsorption spectra

P. Recanatini, P. Nicolosi,* and P. Villoresi

Dipartimento di Elettronica e Informatica, Università di Padova, Istituto Nazionale per la Fisica della Materia, Unità di Padova, via Gradenigo 6/A, 35131 Padova, Italy

(Received 28 November 2000; published 15 June 2001)

The photoabsorption spectrum of C II, from the ground and 4P first excited levels, has been studied with the dual laser plasma technique. Both the discrete spectrum due to bound-bound transitions and the photoionization continua have been observed. Accurate wavelength measurements have been performed and new lines have been identified. Furthermore, relative oscillator strength values have been derived. The photoionization cross sections have been measured in relation to the oscillator strengths of the discrete transitions, and several resonances, showing characteristic Fano profiles, have been observed too. Experimental data have been compared with theoretical calculations.

DOI: 10.1103/PhysRevA.64.012509

PACS number(s): 32.30.Jc, 32.80.Dz, 32.80.Fb

I. INTRODUCTION

Knowledge of photoionization cross sections and absorption oscillator strengths is fundamental for the modeling and diagnosing of both astrophysical and laboratory plasmas. For this reason, a great effort has been devoted in order to derive accurate atomic parameters of several elements of astrophysical interest in any ionization stage. In particular, considerable theoretical work has been done in recent years that consistently improves the quality of computed data. To this purpose, the studies within the OPAL [1], Opacity [2], and Iron [3,4] Projects deserve mentioning. Nevertheless, the experimental measurement of atomic parameters is still relatively scarce mainly in the case of charged atomic states. One well-established technique for the study of atomic spectra is absorption spectroscopy. However, whereas various experiments have been performed in the case of neutral atoms, very few experimental data have been reported for ions. The reason is mainly related to the difficulty in generating a suitable column of absorbing ions. One well-established technique uses two laser-produced plasmas, one acting as a source of background spectrally continuous radiation, the other as an absorbing medium [5,6]. The peculiar properties of laser-generated plasmas allow us to get a high brightness source of extreme ultraviolet (EUV) and soft x-ray (XUV) radiation with uniform spectral distribution by sharply focusing laser pulses on targets of high atomic number materials. This source is used to irradiate a further absorbing plasma. Since in a laser plasma the various ionic states have different time evolution and spatial distributions, a good selection among different ion charge states can be obtained by introducing a suitable delay between the generation of the two plasmas and focusing the EUV background radiation on the absorbing plasma with good spatial resolution; in addition to this, the very short duration of emission from the plasma source, which has the duration of the laser pulse, about 20 ns [7], is fundamental to freezing the spectroscopic evolution of the plasma.

This paper, which follows a Brief Report on some preliminary measurements by Nicolosi and Villoresi [8], pre-

sents a measurement of the absorption spectrum of C II performed by the above-mentioned dual laser plasma technique.

Theoretical data on C II have been published by several authors who have used different computational approaches [9–17]. In particular, Yan and Seaton [11] and Yan, Taylor, and Seaton [12] calculated atomic data for the photoionization cross sections and oscillator strengths by using close-coupling methods. The photoionization cross-section calculations have been revised by Vo Ky Lan *et al.* using two different computer codes [13]. More recently, calculations have been performed by Nahar and Pradhan [4,16,17] within the Iron Project. These latter are performed with the same close-coupling approximation and using *R*-matrix methods such as those carried out within the Opacity Project, but a larger basis set and a finer energy resolution have been used.

The C^+ photoionization cross section has been measured by the dual laser plasma technique by Nicolosi and Villoresi [8]. They have measured the photoabsorption spectrum from 70 to 40 nm. Both discrete transitions below the ionization limit and resonances above it have been measured and new terms have been identified. The absolute C II photoionization cross section from the ground level has been recently measured by Kjeldsen *et al.* [18] using synchrotron radiation with an ion beam in the region around the first threshold.

The present results extend considerably the previous measurements. Both the photoabsorption spectra from the ground, $^2P^o$, and first excited level, 4P , have been measured. The signal-to-noise ratio of the acquired data has been significantly improved compared to previous measures. This allowed a high spectral resolution and experimental accuracy. Spectral identification of the observed transitions with accurate wavelength measurements have been performed. The relative values of the absorption oscillator strengths of discrete transitions have been derived and the absolute value of the photoionization cross sections has been deduced from the oscillator strength values. Furthermore, spectral profiles of resonances have been clearly resolved and the measurement of the photoionization cross section has been extended up to 32 nm.

II. DESCRIPTION OF THE EXPERIMENT

The experiment has been described in detail in [19]. We would like to give the essential elements useful for a com-

*Email address: nicolosi@dei.unipd.it

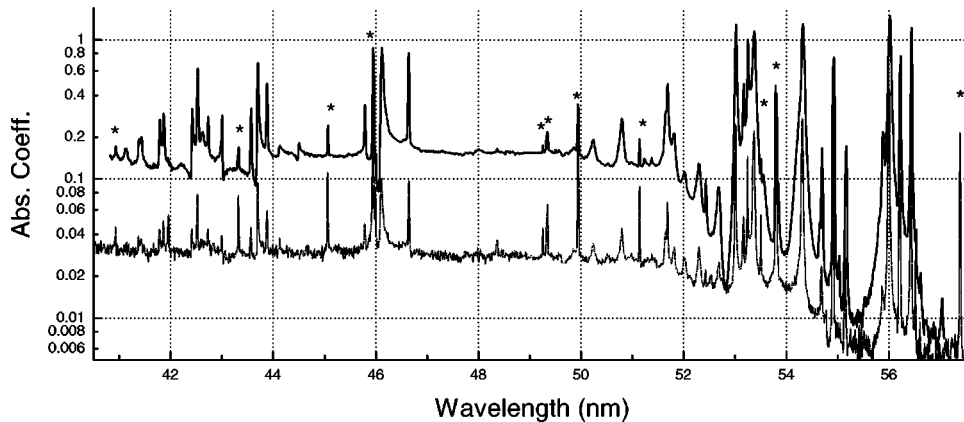


FIG. 1. Absorption coefficient spectra of C II between 40.8 and 57.5 nm taken at $y=2.1$ mm (top curve) and $y=3.3$ mm (bottom curve) from the C target. C III lines are indicated with an asterisk.

plete understanding of the measurement.

The beam (5 J, 15 ns) from a Nd-YAG (yttrium aluminum garnet) laser (Q -Switched and injection seeded for single longitudinal mode (SLM) operation) was split into two parts. About 3.8 J of the laser pulse energy was sharply focused, using a best form spherical lens ($f=100$ mm), onto a tungsten (W) target generating the plasma (BR) backradiator. The remaining energy, 1.2 J, was focused onto a graphite (C) plane target in order to generate the absorbing plasma column (PC).

The W plasma was stigmatically imaged onto the entrance slit of a normal incidence spectrograph via a toroidal mirror ($R=1259.8$ mm, $\rho=1040.7$ mm, Pt coated, working at angle of incidence 24.6°). The W target was oriented 45° both respect to the incoming laser beam and to the line of sight of the spectroscopic apparatus. In such a way, the high-density, high-temperature laser-target interaction region, corresponding to the brightest emitting plasma, was imaged [20]. The C target was placed in front of and close to (at about 6 mm) the entrance slit of the spectrograph. Its surface was oriented perpendicular to the length of the slit, consequently only a small portion of the expanding C plasma was irradiated by the BR plasma. The size of the probed region was about 0.35 mm wide parallel to the target surface, while along the slit it was defined by the imaging properties of the spectrograph and by the characteristics of the detector. In addition, by moving the target it was possible to probe the plasma in different regions while the time of the probing was suitably optimized by delaying the generation of the W plasma, with respect to the C one, by varying the length of an optical delay line. Finally, the laser beam was focused on the C target with a spherocylindrical lens to obtain an elongated plasma column (focal spot 0.1×9 mm²), thus increasing the length of the absorbing medium.

The spectrum was analyzed via a normal incidence stigmatic spectrograph, mounting a toroidal grating ($R=1011.1$ mm, $r=991.8$ mm, Pt coated) with 3600 lines/mm. The detector was a two-dimensional CCD (512×512 square pixels of $24 \mu\text{m}$) with uv-enhanced response and 16-bit readout, supplied by Princeton Instruments. It was operated at -30°C , which resulted in the best compromise to get a low thermal noise and a negligible reduction of detection efficiency due to contaminant layer condensation on the detector surface. It was mounted in a fixed position on the focal Row-

land surface of the spectrograph. The corresponding dispersion was 6.6 pm/px, so a spectral interval of about 3.3 nm was recorded for each exposure. The spectrum was scanned by moving the grating, which was mounted on a rotating arm, pivoted at the center of the Rowland circle, and whose length was equal to the radius of the latter. The experimental spectroscopic apparatus has been fully characterized with dedicated spectroscopic observations of laser-generated plasmas, by which it has been verified that the residual aberrations give an instrumental function, along the spectral dispersion direction, well fitted by a Lorentzian curve of about 2.4 pixels width [19]. The pixel size is projected onto the plasma with a magnification ratio of about 1:1, thus defining the size of the probed plasma in the sagittal plane, as already stated.

Serrated-edge apertures have been used in the laser system in order to reduce diffraction affecting the intensity distribution of the laser beam, in particular for long path lengths. Moreover, with the apertures, a portion around the maximum of the intensity distribution of the output pulse from the laser oscillator was selected; in this way, gain saturation in the final amplifier stages and correspondingly a more reproducible shot to shot intensity distribution was obtained. Consequently, a considerable improvement of the acquired data in terms of signal-to-noise ratio has been obtained. This is clear if one compares the spectra in Fig. 1 with that reported in the previous paper [8].

III. EXPERIMENTAL RESULTS

The absorption spectrum of C II between 40.8 and 57.5 nm is shown in Fig. 1. It has been taken under the following experimental conditions: time delay about 58 ns, laser beam energy about 1.2 J, focused in an elongated spot of about 9 mm.

About 20–30 exposure sequences have been added for each 3.3-nm-wide spectral interval recorded by the CCD detector. In the figure, the absorption coefficients of two spectra are shown. They have been taken by probing the absorbing plasma at distances, respectively, of 2.1 and 3.3 mm from the target, while keeping the other experimental parameters unchanged. Shorter distances from the graphite target correspond to higher column densities, and so they have been chosen in order to measure absorption features corresponding to small oscillator strengths or cross sections. In both spectra, discrete absorption lines are evident; they cor-

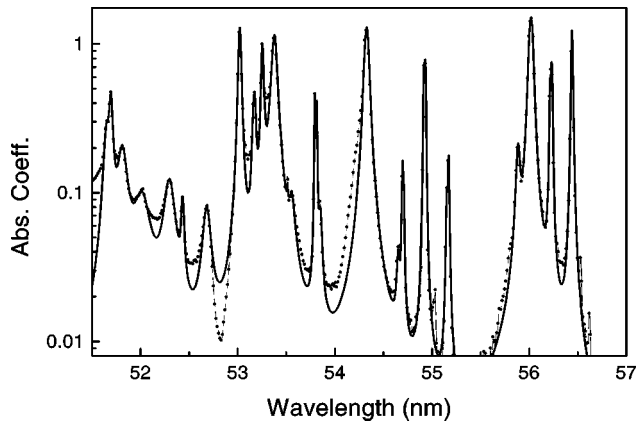


FIG. 2. Example of the synthesis of the absorption spectrum in the 51.5–56.5-nm band. Continuous curve, synthetic spectrum; line-dotted curve, experimental spectrum.

respond to $2s^22p^2\ ^2P^o-2s^2nd\ ^2D$ and $2s^22p^2\ ^2P^o-2s^2ns\ ^2S$ transitions from the ground level and also to $2s2p^2\ ^4P-2s2p(^3P)nd\ ^4D^o$, $^4P^o$, $ns\ ^4P^o$ from the first excited level. The resonance series, 2D and 2S , from the ground level converge to a common limit at about 50.8 nm. In addition to this, the 2D series shows a clear discontinuity in the smooth trend of relative absorption coefficients between the $n=7$ and $n=8$ terms, due to the $2s2p(^3P)3p\ ^2D$ perturbing term. The 2S series has been observed only up to the $n=6$ term; the following one $n=7$ at about 53.87 nm is merged with a strong C III line and it corresponds to the spectral feature on the red wing of the profile of this line (see also Fig. 2). On the other hand, the series from the 4P metastable level converge to a limit at about 48.5 nm and in fact a small jump appears superimposed to the continuous absorption from the ground level. The continuous absorption spectrum extends beyond the photoionization thresholds and several resonances are evident with typical Fano-type profiles.

Some residual C III absorption is present, with a few absorption lines indicated with an asterisk throughout the spectrum. This shows that the selection of the C II ionization stage with respect to the adjacent ones has not been fully accomplished. Indeed the ionization energy of C I is 11.26 eV while that of C II is only slightly larger, 24.38 eV.

The semilogarithmic scale in Fig. 1 has been chosen in order to clearly show the weakest spectral features. In fact, the jumps at threshold of the photoionization from both the $^2P^o$ ground and the 4P metastable level are clearly evident, as well as very weak absorption lines. The signal-to-noise ratio of the reported spectra is very impressive; only in the spectrum recorded at 3.3 mm from the graphite target does some noise affect the lowest absorption coefficient values. In addition to this, some residual statistical fluctuations of the absorption coefficient between the various adjacent spectral intervals, which have been joined to compose the full spectrum, have not been averaged out, and can be seen throughout the spectrum as small discontinuities of the absorption coefficient. However, they correspond to very small absolute values, comparable with the noise level. In addition to this, it is interesting to note that the absorption lines of C III are

relatively stronger than those of C II compared to the spectrum taken closer to the C target. This can be explained by taking into account that probing the plasma at larger distances from the target, while keeping constant the delay from the generation of the carbon plasma, corresponds to testing the species that move faster or alternatively testing the plasma at earlier times. In this way, the ionization stages with higher charge are favored. This characteristic is useful also in discriminating lines with doubtful assignment.

In the continuous spectra, beyond the ionization limit, the series corresponding to $2s^22p^2\ ^2P^o-2s2p(^3P^o)np\ ^2D$, 2S , 2P transitions are evident. The first two can autoionize and show typical resonance shapes while autoionization is forbidden by the selection rules for the third one and correspondingly the lines have narrow spectral features.

In order to derive the relative distribution of the oscillator strengths of the various transitions and to extend it to the continuous photoabsorption cross section, as will be explained later on, we have performed a synthetic fit of the observed spectra. In fact, the transitions are not isolated, on the contrary they appear in general in composite spectral features, which are partially merged with other ones.

Indeed, although the spectral resolution is relatively quite high, one detector pixel corresponding to about 0.0066 nm, the lines show spectrally broadened profiles mainly due to plasma density effects, such as Stark broadening. Other broadening effects, namely thermal Doppler and motional Doppler, should be negligible, the first one because after the long delay the plasma temperature has dropped considerably, the second one because the cylindrical focusing geometry of the laser beam favors transverse expansion of the plasma, which reduces the velocity components along the line of sight of the spectroscopic system.

Furthermore, the synthetic fit of the spectral line profiles has allowed more accurate definition of their relative separation and correspondingly reliable wavelength measurements.

The synthetic fit has been applied to the absorption coefficient spectrum, $k(\lambda)$, which should be proportional to the intrinsic profile of the considered spectral line. Each spectral line has been fitted using Lorentzian profiles of constant width for the various fine-structure components and scaling their area according to the relative gf values. The resulting profile has been assumed as representative of the experimental spectral feature as if it had been isolated. In Fig. 2, an example of the synthetic fit applied to the spectrum, taken at 2.1 mm, between 51.5 and 56.5 nm is reported. The fit appears definitely quite good, with only some slight differences evidenced in the log-scale plot. In any case, the estimated resulting area of some profiles is affected by only a few percent.

A. Spectral identifications

Emission and absorption lines, both of C II and III, whose wavelengths have been measured with high accuracy and are reported in the literature [21], have been used as standards. A polynomial fit of the dispersion function of the grating has been determined by minimizing the deviation of the predicted wavelengths from the standard values. In Table I, the

TABLE I. New absorption lines identified below the photoionization jump.

Transitions	Meas. λ (nm)	Calc. λ (nm)
$2s^22p \ ^2P^o-2s^27s \ ^2S$	53.864	53.875
$2s^22p \ ^2P^o-2s^28d \ ^2D$	52.696	52.700
$2s2p^2 \ ^4P-2s2p(^3P^o)6s \ ^4P^o$	52.446	52.444
$2s^22p \ ^2P^o-2s^29d \ ^2D$	52.310	52.309
$2s^22p \ ^2P^o-2s^210d \ ^2D$	52.031	52.025
$2s^22p \ ^2P^o-2s^211d \ ^2D$	51.826	51.816
$2s^22p \ ^2P^o-2s^212d \ ^2D+2s2p^2 \ ^4P-2s2p(^3P^o)6d \ ^4P^o$	51.665	51.659
$2s2p^2 \ ^4P-2s2p(^3P^o)7d \ ^4D^o+^4P^o$	50.807	50.812/50.786
$2s2p^2 \ ^4P-2s2p(^3P^o)8d \ ^4D^o+^4P^o$	50.248	50.253/50.236
$2s2p^2 \ ^4P-2s2p(^3P^o)9d \ ^4D^o+^4P^o$	49.870	49.878

new lines, corresponding to relatively high members of the series from both the ground and the first excited level, have been listed with their identifications, the measured wavelengths, and the calculated ones. The latter have been derived by extrapolating the quantum defect along the Rydberg series. The reported measured wavelength values have been averaged among several independent measurements, derived from spectra taken in different experimental sessions. The experimental accuracy, taking into account some residual systematic deviation due to the polynomial approximation of the grating dispersion curve, has been estimated to be about 0.005 nm, i.e., just below the spectral size corresponding to one detector pixel. This is the accuracy also for the other wavelength measurements that will be reported further on, unless specified differently. The reported values improve the preliminary measurements reported in [8], however the relative difference is within the experimental uncertainties; in the $8d \ ^4D, ^4P$ terms it is slightly larger, but in that case the signal-to-noise ratio of the earlier data was relatively poor. Furthermore, for the sake of completeness, we should note that the wavelength value given for the transitions $2s2p^2 \ ^4P-2s2p(^3P^o) \ 9d \ ^4P^o+^4D^o$ has been derived from only two measurements and consequently it has a higher uncertainty. This is also true for the $2p-7s$ line, which appears merged with other ones.

The series $2s^22p-2s^2nd$ has been followed up to the term with $n=12$ while the $2s2p^2 \ ^4P-2s2p(^3P)nd \ ^4P^o, ^4D^o$ up to $n=9$. As stated above, both the 2D and 2S series are perturbed, the first by the $2s2p(^3P)3p \ ^2D$ and the second by the $2s2p(^3P)3p \ ^2S$ terms, and the effect of the perturbation is evident in the former case for terms with n greater than 7, while only the first few terms of the weaker 2S series have been observed.

In Table II, the new lines identified beyond the ionization threshold are reported. Identifications have been based on the calculations reported in Refs. [8,9,22,23] and on extrapolations along the Rydberg sequences. These identifications will be discussed in more detail further on in the analysis of the photoionization cross section. The wavelength measurements of resonances correspond to the peak of the absorption profile, which has been measured with higher accuracy than the resonance wavelength determined by the fitting of the spectral feature with Fano-type profiles. The series

$2s^22p \ ^2P^o-2s2p(^3P^o)np \ ^2D, ^2S, ^2P$ have been followed nearly up to the second limit $2s2p(^3P^o)$ at about 40.2 nm. The continuous spectrum of k also has a contribution from the photoionization of ions on the first excited level $2s2p^2 \ ^4P$; in fact, this level is metastable, so some population can concentrate on it and, besides these, the corresponding cross section, is about twice that from the ground state. Indeed, the series $2s2p^2 \ ^4P-2s2p(^3P^o)nd \ ^4P^o, ^4D^o$ converge to the corresponding threshold of the photoionization cross section, as can be clearly observed at about 49 nm in Fig. 1. Moreover, the resonances due to transitions $2s2p^2 \ ^4P-2p^2(^3P)np \ ^4D^o, ^4P^o$ ($n=3$) at about 44.5 and 44.1 nm have been identified. The higher members of this series, $n>3$, can be clearly identified in Fig. 4, at about 38.9 and 36.9 nm, although they appear quite weak. Unfortunately, they are merged with strong C III lines.

In Table III, some unidentified lines are reported. These lines can be definitely attributed to C II. In fact, in spectra taken at different distances from the target, they follow the

TABLE II. Transitions beyond the ionization threshold. The calculated values are only those extrapolated by authors.

Transitions	Meas. λ (nm)	Calc. λ (nm)
$2s^22p \ ^2P^o-2s2p(^3P^o)4p \ ^2D$	46.118	
$2s^22p \ ^2P^o-2s2p(^3P^o)4p \ ^2S$	45.796	
$2s2p^2 \ ^4P-2p^2(^3P)3p \ ^4D^o$	44.512	
$2s2p^2 \ ^4P-2p^2(^3P)3p \ ^4P^o$	44.130	
$2s^22p \ ^2P^o-2s2p(^3P^o)5p \ ^2D$	43.711	
$2s^22p \ ^2P^o-2s2p(^3P^o)5p \ ^2S$	43.577	
$2s^22p \ ^2P^o-2s2p(^1P^o)3p \ ^2D$	43.010	
$2s^22p \ ^2P^o-2s2p(^3P^o)6p \ ^2P$	42.738	42.752
$2s^22p \ ^2P^o-2s2p(^3P^o)6p \ ^2S$	42.627	
$2s^22p \ ^2P^o-2s2p(^1P^o)3p \ ^2P$	42.535	
$2s^22p \ ^2P^o-2s2p(^3P^o)6p \ ^2D$	42.423	42.420
$2s^22p \ ^2P^o-2s2p(^3P^o)7p \ ^2P$	41.870	41.851
$2s^22p \ ^2P^o-2s2p(^3P^o)7p \ ^2D$	41.794	41.787
$2s^22p \ ^2P^o-2s2p(^3P^o)8p \ ^2P$	41.433	41.421
$2s^22p \ ^2P^o-2s2p(^3P^o)8p \ ^2D$	41.389	41.382
$2s^22p \ ^2P^o-2s2p(^3P^o)9p \ ^2P$	41.145	41.135
$2s^22p \ ^2P^o-2s2p(^3P^o)9p \ ^2D$	41.118	41.101

TABLE III. Unidentified transitions below the second ionization threshold. An asterisk denotes tentative assignment to C II; see the text for details.

No.	λ (nm)
1	55.890
2	54.672*
3	53.573*
4	51.388
5	51.252

same behavior as the other C II lines as opposed to those of C III, although some of them could be due to some density-dependent plasma effect. Furthermore, other lines appearing beyond the second photoionization limit $2s2p^3P^o$, i.e., with wavelength shorter than 40.2 nm, can be easily recognized through careful comparison with the calculated spectrum, which has been superimposed on the experimental one in Fig. 3, although some of them appear merged with relatively strong C III absorption lines.

B. The photoionization continua

In Fig. 3, the absorption coefficient corresponding to the continuous photoionization spectrum, as reported in Fig. 1, is shown enlarged for the spectrum taken at 2.1 mm from the graphite target. There the various resonances are clearly visible. As already discussed, C II has been studied within the Opacity Project and both photoionization cross section and oscillator strengths have been calculated [11,12]. These results have been revised by Lan *et al.* [13] and recently, within the Iron Project, using a larger basis set by Nahar and Pradhan and by Nahar [4,16,17]. The theoretical cross section determined by Yan and Seaton has been superimposed in the figure along with that of Nahar *et al.* It can be clearly

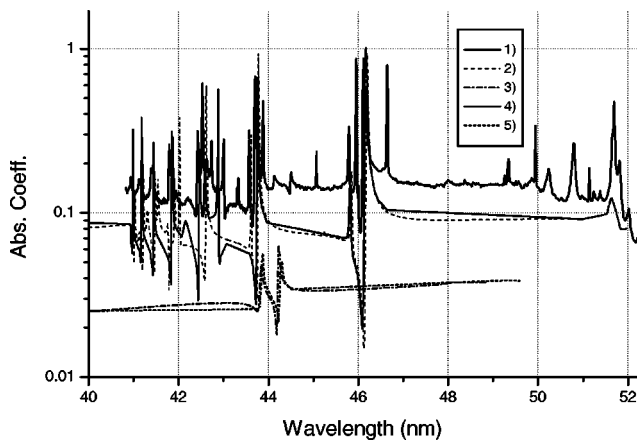


FIG. 3. Photoionization continua between 40 and 52 nm. Curve legend: (1) experimental measurement, (2) calculations relative to ground state from Ref. [16], (3) calculations relative to quartet state from Ref. [16], (4) calculations relative to ground state from Ref. [11], (5) calculations relative to quartet state from Ref. [11]. The computed cross sections have been scaled according to the experimentally derived ion densities.

observed that the former resembles more accurately the experimental spectral features. For comparison purposes, the theoretical cross sections have been convoluted with the instrumental function and scaled with the column densities experimentally derived. Both the cross sections from the ground $^2P^o$ level and from the first excited 4P level have been separately reported, together with that of 4P alone. The agreement with the observed spectrum is impressive, although some discrepancies are present concerning the relative position of the various resonances.

Both edges corresponding to the ionization of the ground ($^2P^o$) level and of the excited (4P) one are clearly distinguishable. In fact, in the window between 48 and 52 nm, the transition from photoexcitation to photoionization relative to the 4P excited level is clearly visible, with the higher members of the discrete series $^4P^o$, $^4D^o$ converging to the limit. Beyond the latter, some resonances can be observed at about 44 nm. These, as already stated, have been identified as $2s2p^2\ ^4P-2p^2(^3P)3p\ ^4D^o$, $^4P^o$ by extrapolating the transition energy along the isoelectronic sequence. Indeed, the energy of these transitions is lower than that of ionization for elements with $Z > 6$ and only for C II is the upper level higher than the ionization limit and can autoionize since the corresponding continuum is $\epsilon p\ ^4P^o, ^4D^o$.

Beyond the previously mentioned thresholds, the continuous spectra due to photoionization extend up to the second $2s2p^3P^o$ threshold, and the smooth transition towards the limit caused by the merging of the lines can be observed at about 41 nm. Unfortunately, because of some mechanical constraints in the spectroscopic apparatus, the exact region corresponding to this limit has not been observed.

However, the photoionization cross section has been followed beyond the second limit up to 32 nm. The spectrum of the absorption coefficient between 32 and 40 nm is shown in Fig. 4. The signal-to-noise ratio is worse than in the previous data. The reason for this is that the background continuous signal was considerably lower because of the short-wavelength cutoff of the efficiency of the spectroscopic system [19]. In addition to this, the absorbing plasma has been probed here at 1.6 mm from the target, corresponding to a higher column density of carbon ions, in order to have a reasonably detectable absorption coefficient. For this reason, these data cannot be directly related to the spectrum shown in Fig. 3. Nevertheless, the calculated spectrum from Ref. [8], corresponding to photoionization from the ground state, has been superimposed by normalizing to the values of k on the long-wavelength side. Furthermore, the theoretical cross section from the first excited level has also been reported. However, since the ratio of ion densities between the ground and excited level is missing, an arbitrary column density value N_I was used for this second curve.

In any case, it is interesting to observe that the various resonances and spectral features foreseen by the theory have been observed, although some of them coincide with absorption lines of C III and consequently are not clearly resolved.

The absolute value of the cross sections below the second limit has been estimated by extracting the column density of the ions on the ionizing levels from the discrete lines of the series converging to the relative limits. The procedure we

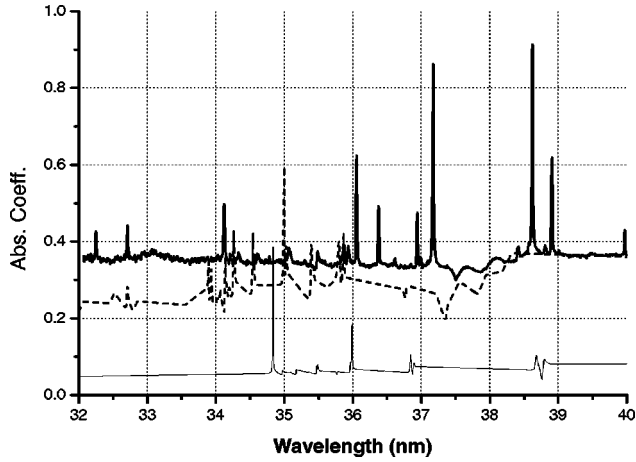


FIG. 4. Photoionization continua beyond the second threshold ($2s2p^3P^o$). Continuous curve, experimental data; dashed curve, 2P ; dotted curve, 4P theoretical cross sections from Ref. [11]. The wavelengths of the transitions of the type $2s2p^2^4P-2p^2(^3P)4,5p^4D^0,^4P^0$, which correspond to the first and second structures in the long-wavelength side of the calculated spectrum, were difficult to determine. Therefore, they are not reported in Table II but are discussed in the text.

have followed is explained in the following section.

C. Oscillator strength and photoionization cross-section measurements

From the synthesis of the absorption spectrum taken at about 3.3 mm, the relative oscillator strengths of the observed lines have been derived. In fact, at this distance from the target, the column density of C ions is not so high as to cause saturation effects in the absorption, and the measured absorbance results are proportional to the absorption oscillator strengths of the related transitions. In Fig. 5, the relative oscillator strengths, experimentally measured, are reported normalized to the one calculated for the $2p-5d$ resonance transition from the ground level. The agreement with the distribution of the computed oscillator strengths is very good, well within the estimated error bars for the members of the series below the perturbation, i.e., up to $n=7$. However, some discrepancies are evident for the higher n members of

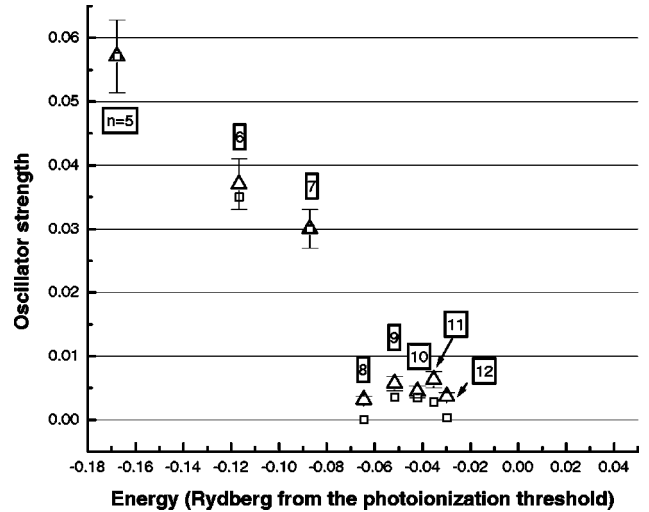


FIG. 5. Experimentally measured oscillator strengths for transition $2p-nd$ from the ground level normalized to that calculated for the $2p-5d$ transition. Open triangles, experimental data; open squares, theoretical data from Refs. [11,22].

the series. Similarly, the oscillator strengths for transitions starting from the excited 4P level have been derived. In Table IV, the oscillator strengths derived in relation to other transitions from the same levels are reported. In particular, the oscillator strengths for transitions originating from the $2p$ ground state have been derived in relation to the average among the $2p-5d$, $-6d$, $-7d$ and $2p-6s$ and $2p^2P^o-2s2p(^3P)3p^2P$ and $-4p^2P$ transitions, while those from the 4P excited level have been determined relative to the average among the $2s2p^2^4P-2s2p(^3P)4d^4P^o,^4D^o$, and $-5d, -5s^4P^o$ transitions. Likewise, the oscillator strengths of the higher members of the resonance series up to $n=12$ have been derived. The major discrepancies with the calculated values have been found in the case of the $2s^22p^2P^o-2s2p(^3P)3p^2D$ and $2s^22p^2P-2s^28d^2D$ transitions: the corresponding experimental oscillator strengths were measured as $f=0.023$ and $f=0.0031$, respectively, while the theoretical values are $f=0.0361$ and $f=0.00004$ [8,16]. The uncertainty in the measured f values has been estimated to be about 10% for the strongest lines and 20% for the weakest, partially due to

TABLE IV. Oscillator strength measurements.

Transitions	Measured λ (nm)	Oscillator strength
$2s2p^2^4P-2s2p(^3P^o)5d^4D^o$	53.268	0.051 ± 0.003
$2s^22p^2P^o-2s2p(^3P^o)3p^2D$	53.034	0.023 ± 0.002
$2s^22p^2P^o-2s^28d^2D$	52.696	0.0031 ± 0.0003
$2s^22p^2P^o-2s^29d^2D$	52.310	0.0054 ± 0.0005
$2s^22p^2P^o-2s^210d^2D$	52.031	0.0041 ± 0.0004
$2s^22p^2P^o-2s^211d^2D$	51.826	0.0059 ± 0.0006
$2s2p^2^4P-2s2p(^3P^o)6d^4D^o$	51.706	0.025 ± 0.0016
$2s^22p^2P^o-2s^212d^2D$	51.665	0.0034 ± 0.0004
$2s2p^2^4P-2s2p(^3P^o)7d^4D^o+^4P^o$	50.807	0.019 ± 0.0012
$2s2p^2^4P-2s2p(^3P^o)8d^4D^o+^4P^o$	50.248	0.015 ± 0.0009

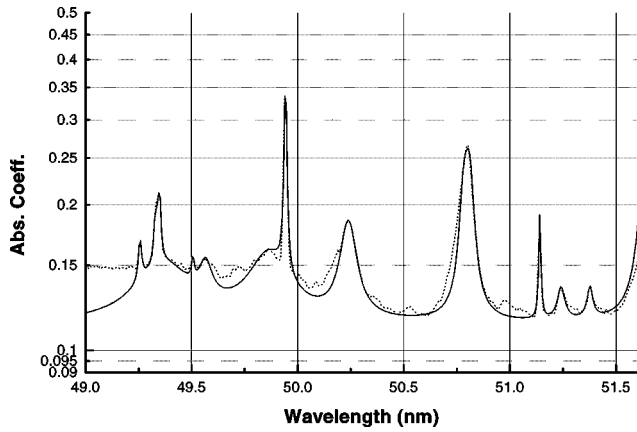


FIG. 6. Synthesis of the absorption coefficient at the 4P photoionization threshold. Dotted curve, experimental data; continuous curve, synthetic spectrum.

the accuracy of the computed values that have been used in the normalization procedure and also to the uncertainty in the synthetic fit of the spectra used to extract the line profiles.

Unfortunately, the spectrum taken at 3.3 mm from the graphite target was not useful in order to derive a measure of the photoionization jump. In fact, the value obtained was comparable to or even less than the overall estimated uncertainty. For this reason, after deriving the relative behavior of the oscillator strengths for the various lines, we took a spectrum closer to the target at about 2.1 mm. In this case, the column density is higher and correspondingly the photoionization jump is measurable with greater accuracy. The corresponding values of the photoionization jumps have been derived through the synthesis of the lines converging to the limit. In Fig. 6 and Fig. 7, the synthesis of the spectrum at the 4P photoionization threshold is reported and the jumps correspondingly derived are shown. The value of the photoionization cross section, $\sigma(\lambda)$, is related to the density of absorbing ions through the following expression:

$$k(\lambda) = \sigma(\lambda)N_l, \quad (3.1)$$

where k is the absorption coefficient and N_l is the so-called column density, i.e., the density of absorbing ions integrated along the absorption path of the background radiation.

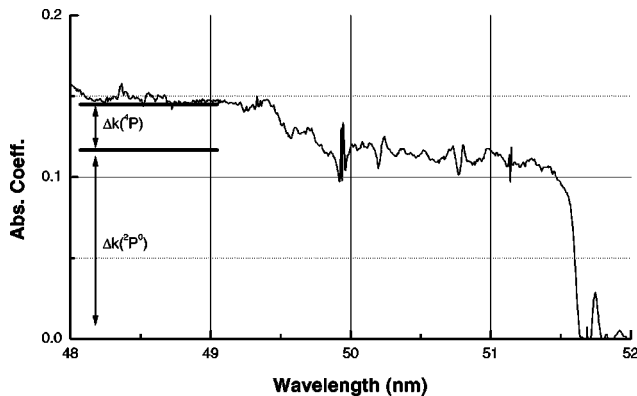


FIG. 7. Difference between the two spectra of Fig. 6.

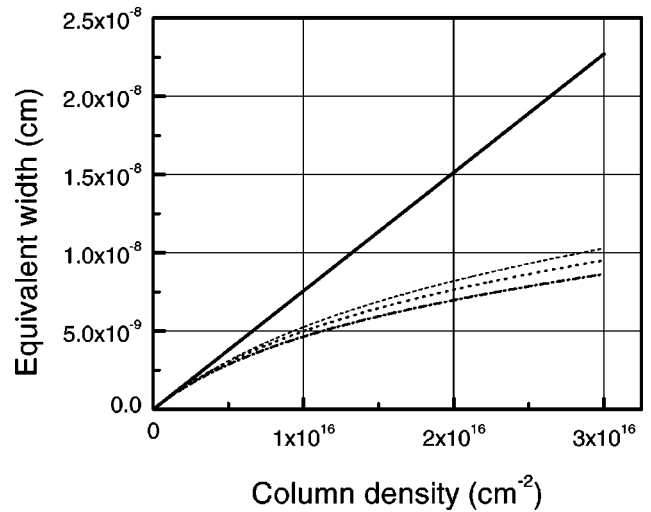


FIG. 8. Equivalent width of the $2s^2 2p^2 P^0 - 2s^2 7d^2 D$ line vs the density of absorbing ions and for spectral widths differing $\pm 10\%$ from the experimentally estimated one. See text for discussion.

In order to derive the column density, we have estimated the equivalent width of the various transitions versus the column density and the spectral width of the line profiles.

The equivalent width is defined by

$$W_\lambda = \int \frac{I_{0\lambda} - I_\lambda}{I_{0\lambda}} d\lambda, \quad (3.2)$$

where

$$I_\lambda = I_{0\lambda} e^{-k_\lambda}. \quad (3.3)$$

It is well known that only for small values of the absorption coefficient is the equivalent width proportional to the oscillator strength of the transition, while for optically thick lines saturation occurs [24]. While this effect is nearly negligible for the weak lines near the ionization limit, this is not the case for the strong resonance lines. In Fig. 8, the equivalent width for the case of the $2s^2 2p^2 P^0 - 2s^2 7d^2 D$ line is reported versus the column density of C ions for three different spectral widths of the line profile derived according to the estimated uncertainty in the synthesis of it. It is clear that for high-density values, the equivalent width deviates from the linear optically thin behavior and, in addition to this, larger spectral widths tend to shift the curve towards the optically thin case. Correspondingly, the lines with lower oscillator strengths and larger spectral width profiles are less affected by saturation. Furthermore, an additional uncertainty must be accounted for those lines whose spectral width is narrower than the instrumental function one. In Tables V and VI, the equivalent width determined for the various transitions, through the described synthesis procedure, is reported with the oscillator strength, the spectral width of the profile, and the derived column density.

In the case of the $2s^2 2p^2 P^0 - 2s^2 2p(3P^0)3p^2 D$, we have assumed the experimentally determined f value. The values of column density on the ground level show a relatively nar-

TABLE V. Equivalent width determined for various transitions from the ground state, with the oscillator strength, the spectral width of the profile, and the derived column density.

Transitions	Equivalent width (10^{-9} cm)	f value	Spectral width (nm)	N_l (10^{16} cm $^{-2}$)
$2s^22p \ ^2P^o-2s^25d \ ^2D$	8.38	0.0571	0.052	1.32
$2s^22p \ ^2P^o-2s^26d \ ^2D$	8.55	0.035	0.055	2.26
$2s^22p \ ^2P^o-2s^27d \ ^2D$	8.90	0.030	0.060	2.60
$2s^22p \ ^2P^o-2s^26s \ ^2S$	6.10	0.00112	0.013	2.34
$2s^22p \ ^2P^o-2s2p(^3P^o)3p \ ^2P$	2.21	0.0182	0.01	1.00
$2s^22p \ ^2P^o-2s2p(^3P^o)3p \ ^2D$	5.19	0.023	0.030	2.54

row distribution with the exception of those corresponding to the $2p-5d$ and $2s^22p \ ^2P^o-2s2p(^3P^o)3p \ ^2P$ transitions. It should be noted that the $2p-5d$ transition has a relatively large oscillator strength, while the latter has a relatively narrow line profile. Similarly, the $2s2p^2 \ ^4P-2s2p(^3P^o)4d \ ^4D^o$, $5s \ ^4P^o$ transitions show the lowest column density among the ones originating from the 4P excited level. Consequently, we have evaluated an average column density by weighing the values derived from the different lines. The weight factors have been set proportional to the inverse of the square root of the oscillator strength, with an additional 0.3 weight factor for those lines spectrally narrower than the instrumental line profile. The column density of ground-state ions is $n = 2.25 \times 10^{16}$ cm $^{-2}$ and that of the 4P level is $n = 3.83 \times 10^{15}$ cm $^{-2}$. The corresponding values of the photoionization cross sections at threshold are $\sigma(2s^22p \ ^2P^o) = 4.7$ Mb ($\pm 20\%$) and $\sigma(2s2p^2 \ ^4P) = 8.6$ Mb ($\pm 25\%$). The estimated uncertainty is due to the spread of the column density measurements and to the measurement uncertainty of the absorption coefficient at threshold. The derived values of cross section do not significantly change (less than a few percent) by taking into account the column densities determined with the higher members of the series, whose oscillator strengths have been experimentally measured in the present work. The comparison with the theoretical data shows a good agreement. But a slightly larger difference remains between the independent experimental measurements [18], however these values are comparable within the corresponding estimated uncertainties.

D. Resonances

As already observed, various resonances appear beyond the photoionization thresholds. Those identified as $2s^22p \ ^2P^o-2s2p \ (^3P^o)np \ ^2D, ^2S$ can autoionize with the

continuum corresponding to photoionization from the ground level, while the 2P terms cannot, because of selection rules. Those identified as $2s2p^2 \ ^4P-2p^2(^3P)np \ ^4D^o, ^4P^o$ autoionize with the continuum relative to photoionization from the 4P metastable level. The spectral profile of some resonances has been fitted with Fano-type profiles, according to the following well-known equation:

$$\sigma = \sigma_b + \sigma_a \frac{(q + \varepsilon)^2}{1 + \varepsilon^2}, \quad (3.4)$$

where σ_b is a background continuum not interacting with the resonance, σ_a is the average interacting continuum, and ε is the energy displacement from the resonance in units of half-width [25]. In particular, since they are not isolated but appear merged with other lines, a synthesis of the various spectral complexes has been performed. The lines that are not autoionizing and/or show very narrow quasymmetric profiles, as in the case of the 2S and 2P resonances, have been fitted with Lorentzian profiles. Furthermore, in the case of spectrally quasioverlapping resonances, the resulting cross section has been derived according to the following expression:

$$\sigma = \sigma_b + \sigma_a \frac{(q_1 + \varepsilon_1)^2}{1 + \varepsilon_1^2} \frac{(q_2 + \varepsilon_2)^2}{1 + \varepsilon_2^2}, \quad (3.5)$$

where the suffixes identify different resonances interacting with the same continuum.

In Figs. 9(a)–9(c), the experimental profiles (at 2.1 mm from the C target) fitted with the synthetic ones are reported for $2s^22p \ ^2P^o-2s2p \ (^3P^o)np \ ^2D, ^2S$, $n = 4, 5, 6$ resonances. Only these first resonances have been considered, since they show strong and relatively wide profiles, which are not

TABLE VI. Equivalent width determined for various transitions from the first excited state, with the oscillator strength, the spectral width of the profile, and the derived column density.

Transitions	Equivalent width (10^{-9} cm)	f value	Spectral width (nm)	N_l (10^{15} cm $^{-2}$)
$2s2p^2 \ ^4P-2s2p(^3P^o)4d \ ^4D^o$	2.89	0.147	0.015	1.64
$2s2p^2 \ ^4P-2s2p(^3P^o)4d \ ^4P^o$	2.40	0.0497	0.016	3.40
$2s2p^2 \ ^4P-2s2p(^3P^o)5s \ ^4P^o$	0.467	0.00647	0.0035	3.07
$2s2p^2 \ ^4P-2s2p(^3P^o)5d \ ^4P^o$	1.95	0.0231	0.033	4.45
$2s2p^2 \ ^4P-2s2p(^3P^o)6s \ ^4P^o$	0.304	0.00311	0.030	4.18

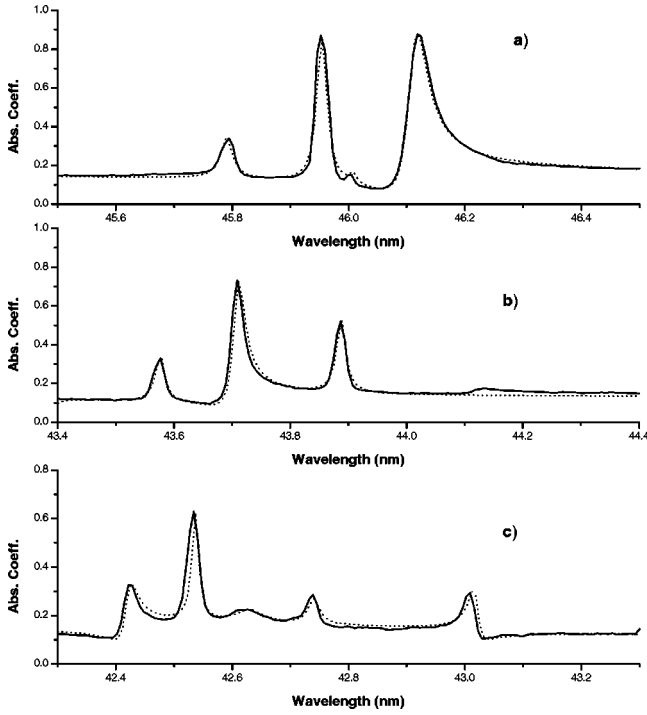


FIG. 9. Details of Fano profiles. Synthesis of $2s^22p^2P^o-2s2p(^3P)np^2D, ^2S$: $n=4$ (a), $n=5$ (b), $n=6$ (c) resonances. The continuous curve is the experimental measurement, the dotted curve is the fitted spectrum.

greatly affected by noise, and are spectrally well separated so that strong interaction effects are nearly negligible and the approximate formula can be used. In Table VII, the resonance wavelength and width $\Delta\lambda$, corresponding to the half-width of the profile and q , characterizing their shape, are reported. The uncertainties of the wavelength can be estimated about 0.09 nm, while for the other two parameters they can be estimated about 30%. The wavelengths of the resonances are systematically shifted with respect to the wavelengths reported in Table II, which correspond to the absorption peaks of the profiles. However, it must be stressed that, as already stated, the uncertainty of the values reported in Table VII are greater than those given in Table II. Finally, the group of lines partially merged between the $2s^22p^2P^o-2s2p(^3P^o)6p^2D$ and the $2s^22p^2P^o-2s2p(^1P^o)3p^2D$ shown in Fig. 9(c) includes the transitions $2s^22p^2P^o-2s2p(^1P^o)3p^2P$, $2s^22p^2P^o-2s2p(^3P^o)6p^2S$, and $2s^22p^2P^o-2s2p(^3P^o)6p^2P$. The assignment of the former two was only tentative in the previous paper, mainly

due to the merging of the lines and the low signal-to-noise ratio. In Ref. [18], the assignment of these lines has been given on the basis of the evaluation of the exchange interaction Slater integrals. In addition to this, we have evaluated, from the fitting of the present spectral features, that the width of the line at 42.5 nm is narrower than that of the instrumental function, while the width of the line at 42.6 nm is 0.05 nm corresponding to about 34 meV. Indeed, the calculations foresee a larger spectral width for this resonance [23]. On the basis of these considerations, we agree with the assignment reported in Ref. [18].

Finally, a broad absorption structure can be observed at 42.212 nm. This value revises the measurement previously reported, which was greatly affected by the very low signal-to-noise ratio. This structure, which is clearly evident in the calculation from the Opacity Project but not in the spectrum computed by Nahar, can be assigned to the $2s^22p^2P^o-2s2p(^1P^o)3p^2S$ resonance whose width is foreseen to be broader than 55 meV. Obviously, the uncertainty of the wavelength measurement, in this case, is greater than that quoted for the data in Table II, due to both the broad spectral profile and to the overlap with nearby resonances, interacting with the same continuum.

IV. CONCLUSIONS

The absorption spectrum of C II from the ground $^2P^o$ state and the first excited 4P state has been measured by the dual laser produced plasmas technique. This measurement extends previously published results. In particular, accurate wavelength measurements have been performed and new terms have been identified in the discrete spectrum as well as beyond the ionization limit. The relative oscillator strengths have been measured and the f values of several new lines have been derived accordingly. The photoionization cross sections both from the ground and from the excited levels have been derived and the results are in good agreement with calculations and independent measurements. The resonances in the continuum have been analyzed and the profiles have been determined according to the Fano theory.

ACKNOWLEDGMENTS

This work has been performed under MURST-Italy contract ‘‘Plasma interaction with nano and picosecond laser.’’

TABLE VII. Resonance Fano profiles parameters: for the estimate of the error, see the text.

Transitions	Resonance λ (nm)	Half-width $\Delta\lambda$ (nm)	q value
$2s^22p^2P^o-2s2p(^3P^o)6p^2D$	42.422	0.006	-2.0
$2s^22p^2P^o-2s2p(^1P^o)3p^2D$	43.019	0.003	2.9
$2s^22p^2P^o-2s2p(^3P^o)5p^2D$	43.705	0.007	-4.6
$2s2p^2^4P-2p^2(^3P)3p^4P^o$	44.122	0.011	-0.95
$2s2p^2^4P-2p^2(^3P)3p^4D^o$	44.505	0.005	-1.7
$2s^22p^2P^o-2s2p(^3P^o)4p^2D$	46.114	0.015	-3.2

- [1] F.J. Rogers and C.A. Iglesias, *Science* **263**, 50 (1994).
- [2] Opacity Project Team, *The Opacity Project*, Vol. 1 (Bristol Institute of Phys., 1995).
- [3] D.G. Hummer, K.A. Berrington, W. Eissner, K.A. Pradhan, H.E. Saraph, and J.A. Tully, *Astron. Astrophys.* **279**, 298 (1993).
- [4] S.N. Nahar and K.A. Pradhan, *Phys. Rev. A* **49**, 1816 (1994).
- [5] P. Nicolosi, E. Jannitti, and G. Tondello, *J. Phys. IV* **1**, 89 (1991).
- [6] J.T. Costello, J.P. Mosnier, E.T. Kennedy, P.K. Carroll, and G. O'Sullivan, *Phys. Scr.* **T34**, 77 (1991).
- [7] P.K. Carroll, E.T. Kennedy, and G. O'Sullivan, *Appl. Opt.* **19**, 1454 (1980).
- [8] P. Nicolosi and P. Villorresi, *Phys. Rev. A* **58**, 4985 (1998).
- [9] R.P. McEachran and M. Cohen, *J. Quant. Spectrosc. Radiat. Transf.* **27**, 111 (1982).
- [10] K.A. Berrington and M.J. Seaton, *J. Phys. B* **18**, 2587 (1985).
- [11] Yu Yan and M.J. Seaton, *J. Phys. B* **20**, 6409 (1987).
- [12] Yu Yan, K.T. Taylor, and M.J. Seaton, *J. Phys. B* **20**, 6399 (1987).
- [13] Vo Ky Lan, M. Le Dourneuf, N.L. Allard, H.E. Saraph, and W. Eissner, *Comput. Phys. Commun.* **55**, 303 (1989).
- [14] K.A. Berrington, W.B. Eissner, H.E. Saraph, M.J. Seaton, and P.J. Storey, *Comput. Phys. Commun.* **44**, 105 (1989).
- [15] L. Quigley and K. Berrington, *J. Phys. B* **29**, 4529 (1996).
- [16] S.N. Nahar and A.K. Pradhan, *Ap. J. Suppl. Ser.* **111**, 339 (1997).
- [17] S.N. Nahar, *Ap. J. Suppl. Ser.* **101**, 423 (1995).
- [18] H. Kjeldsen, F. Folkmann, J.E. Hansen, H. Knudsen, M.S. Rasmussen, J.B. West, and T. Andersen, *Ap. J.* **524**, L143 (1999).
- [19] P. Villorresi, P. Nicolosi, and M.-G. Pelizzo, *Appl. Opt.* **39**, 85 (2000).
- [20] C. Breton and R. Papoular, *J. Opt. Soc. Am.* **63**, 1225 (1973).
- [21] R.L. Kelly, *J. Phys. Chem. Ref. Data Suppl.* **16**, Suppl. 1 (1987).
- [22] W.L. Wiese, J.R. Fuhr, and T.M. Deters, *J. Phys. Chem. Ref. Data Monogr.* **7** (1995).
- [23] K.A. Berrington (private communication).
- [24] L.H. Aller, *Astrophysics—The Atmospheres of the Sun and Stars* (The Ronald Press Co., New York, 1963), p. 300; E.W. Foster, *Rep. Prog. Phys.* **27**, 469 (1964); A. Corney, *Atomic and Laser Spectroscopy* (Clarendon Press, Oxford, 1977).
- [25] U. Fano and J.W. Cooper, *Phys. Rev.* **137**, A1364 (1965).